available at www.sciencedirect.com
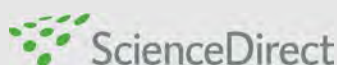
ScienceDirect

journal homepage: www.elsevier.com/locate/chnjc

Article (Dedicated to Professor Yi Chen on the occasion of his 80th birthday)

Selection of oxide supports to anchor desirable bimetallic structures for ethanol reforming and 1,3-butadiene hydrogenation

Tiefeng Wang [a,*], William Lonergan [b], Jingguang G. Chen [c,#]

[a] Beijing Key Lab of Green Chemical Engineering, Department of Chemical Engineering, Tsinghua University, Beijing 100084, China
[b] Center for Catalytic Science and Technology (CCST), Department of Chemical and Biomolecular Engineering, University of Delaware, Newark, DE 19716, USA
[c] Department of Chemical Engineering, Columbia University, New York, NY 10027, USA

ARTICLE INFO

ABSTRACT

Ethanol reforming and 1,3-butadiene hydrogenation reactions were studied on Pt-Ni bimetallic and monometallic catalysts supported on several supports, including γ-Al_2O_3, SiO_2, TiO_2, CeO_2, and high surface area (HSA) and low surface area (LSA) ZrO_2, to elucidate the effect of oxide supports on the bimetallic structures and catalytic activity. The catalysts were prepared by co-impregnation and were characterized by pulse CO chemisorption, transmission electron microscopy, and extended X-ray absorption fine structure. Reactions were carried out in a Fourier transform infrared batch reactor. The supports strongly affected the catalytic activity. For ethanol reforming, the activities of the Pt-Ni bimetallic catalysts were in the order $TiO_2 > SiO_2 > \gamma$-$Al_2O_3 \approx$ LSA-$ZrO_2 > CeO_2 >$ HSA-ZrO_2; while for 1,3-butadiene hydrogenation, the order was $SiO_2 > CeO_2 > \gamma$-$Al_2O_3 >$ LSA-$ZrO_2 >$ HSA-$ZrO_2 \approx TiO_2$. For the hydrogenation reaction, the Pt-Ni bimetallic catalysts outperformed the Pt and Ni monometallic catalysts; in contrast, for the reforming reaction, synergetic bimetallic effects were only found on SiO_2, TiO_2, and HSA-ZrO_2.

1. Introduction

SBimetallic catalysts are used in many reactions such as hydrogenation, dehydrogenation, and reforming because their properties are often different from those of the corresponding monometallic catalysts [1–3]. Many experimental and theoretical studies have been performed to determine the activity and stability of bimetallic systems on well-defined single crystal surfaces [3–5]. The bimetallic structure strongly affects catalytic performance. For example, the Ni-terminated bimetallic surface, with a monolayer of Ni atoms located on a Pt(111) surface, is characterized by increased interactions with adsorbates and is more active for oxygenate reforming than either of the parent metals [6–8]. In contrast, the Pt-terminated bimetallic surface, with Ni atoms located underneath the Pt(111) surface, shows a novel low-temperature hydrogenation pathway that is absent on either Pt(111) or Ni(111) [5]. These surface science results have been extended to γ-Al_2O_3 supported Pt-Ni bimetallic catalysts for hydrogenation reactions, where Pt-terminated bimetallic catalysts show higher hydro-

genation activity than either of the monometallic catalysts [9,10].

The thermodynamically preferred configuration of the Pt-Ni bimetallic catalyst depends on the reaction environment. The Pt-terminated configuration is stable in vacuum or under a hydrogen environment; however, in the presence of adsorbed atomic oxygen, Ni atoms segregate to the surface to produce the Ni-terminated configuration [4]. The interactions between the metals and the support may also affect the configuration of the Pt-Ni bimetallic catalyst, which in turn should affect the catalytic activity for specific reactions.

Supported catalysts often exhibit different catalytic performance, depending on the nature of the support materials. For hydrogenation activity of acetone over Pt/Ni, Qi et al. [11] found that Pt-Ni/SiO_2 bimetallic catalysts exhibited significantly higher activity than Pt-Ni/γ-Al_2O_3 and Pt-Ni/TiO_2. For reforming reactions, Menezes et al. [12] found that Pt/MgO and Pt/ZrO_2 presented better activity than Pt/Al_2O_3 and Pt/CeO_2, and correlated this effect to the strong electron-donating character of MgO and ZrO_2.

In our previous work, TiO_2 and γ-Al_2O_3 were used to study the effect of oxide supports on stabilizing desirable Pt-Ni bimetallic structures for hydrogenation and reforming reactions [13]. In the current study, ethanol reforming and 1,3-butadiene hydrogenation were used as the probe reactions to further study the effects of other oxide supports for Pt-Ni bimetallic catalysts. The oxide supports were TiO_2, γ-Al_2O_3, SiO_2, CeO_2, and ZrO_2 (both high surface area ZrO_2 (HSA-ZrO_2) and low surface area ZrO_2 (LSA-ZrO_2)). We found that the oxide supports strongly affected the catalytic activity, and that the effects were different for reforming and hydrogenation reactions. The supported catalysts were characterized using transmission electron microscopy (TEM) and extended X-ray absorption fine structure (EXAFS) measurements to better understand the differences in activity.

2. Experimental

2.1. Catalyst preparation

The catalysts were prepared by impregnation methods. The supports, γ-Al_2O_3 (surface area: 80–120 m^2/g), amorphous SiO_2 (175–225 m^2/g), CeO_2 (35–45 m^2/g), HSA-ZrO_2 (100–200 m^2/g), LSA-ZrO_2 (20–30 m^2/g), and amorphous anatase TiO_2 (180–300 m^2/g), were purchased from Alfa Aesar. The X-ray diffraction (XRD) patterns of the LSA-ZrO_2 and HSA-ZrO_2 supports were reported in our previous paper [14]. The γ-Al_2O_3, SiO_2, and CeO_2 supports had standard XRD patterns. Precursor solutions were made by adding the necessary volume of deionized water to Pt(NH$_3$)$_4$(NO$_3$)$_2$ (Alfa Aesar) and Ni(NO$_3$)$_2$·6H$_2$O (Alfa Aesar) precursor salts. For high surface area supports (γ-Al_2O_3, SiO_2, HSA-ZrO_2, TiO_2), incipient wetness impregnation was used, while, for low surface area supports (CeO_2, LSA-ZrO_2), slurry phase impregnation was used. All the bimetallic catalysts were synthesized using co-impregnation. After impregnation, the catalysts were dried at 373 K for 10 h and then calcined at 563 K for 2 h. For the monometallic catalysts,

the metal weight loading was 1.7% Pt or 1.5% Ni. For the bimetallic catalysts, the loadings were 1.7% Pt and 1.5% Ni, corresponding to a Pt:Ni atomic ratio of 1:3.

2.2. Catalyst characterization

2.2.1. Pulse CO chemisorption

To determine the number of active sites available on the catalyst, CO uptake was measured using an AMI-200ip (Altamira Instruments, Pittsburgh, USA). Approximately 100 mg catalyst was loaded into a quartz reactor and reduced under 50% H_2/He mixture (40 mL/min) at 723 K for 1 h. After cooling in He, pulse CO chemisorption was performed at room temperature using pulses of 37 cm^3/min CO in a He carrier gas. A thermal conductivity detector (TCD) was used to monitor the flow of CO out of the quartz reactor. Metal dispersion was calculated assuming a stoichiometry of M:CO = 1:1 (M = Pt, Ni).

2.2.2. TEM

TEM analysis was performed using a JEOL 2010F equipped with a Schottky field emission gun operated at 200 keV. Imaging was performed in scanning mode using a 20 nm camera length and a 0.5 nm diameter nanoprobe. Reduced catalyst samples were prepared by grinding and suspending the catalysts in ethanol, followed by dropping a small amount of this solution onto a carbon-coated copper grid. The grid was allowed to dry before loading the sample into the TEM.

2.2.3. EXAFS

To confirm the presence of Pt-Ni bimetallic bonds, EXAFS measurements of the Pt L$_{III}$-edge were performed on the X18B and X19A beamlines at the National Synchrotron Light Source (NSLS), Brookhaven National Laboratory, USA. The catalysts were reduced under 5% H_2/He flow (40 mL/min) at 723 K for 1 h, and data were collected at room temperature. The incident and transmitted X-ray signals were collected with ionization chambers while the fluorescence signal was collected using a 12-channel germanium detector. The EXAFS spectra from the samples were calibrated to the Pt L$_{III}$-edge energy from a Pt reference foil collected in transmission mode. Details of the data analysis were reported in our previous work [9].

2.2.4. In-situ Fourier transform infrared (FT-IR) batch reactor

FT-IR spectroscopy was used to monitor the gas-phase concentrations of reactants and products during reaction. Spectra were recorded at a resolution of 4 cm^{-1} using a Thermo Nicolet Nexus 470 spectrometer equipped with a mercury cadmium telluride (MCT-A) detector. The procedures for preparing samples, details of the sample holder, and the reduction conditions have been previously reported [9]. For each reaction experiment, ~25 mg of the supported catalyst was loaded into the IR cell. The catalyst was reduced by 30 Torr H_2 at 723 K. The details of the reduction were reported elsewhere [13].

For ethanol reforming, ethanol vapor and water vapor were mixed at a partial pressure ratio of 1:3, corresponding to the stoichiometry of ethanol reforming, $C_2H_5OH + 3H_2O \rightarrow 2CO_2 + 6H_2$. To start the reaction, the reactant gas mixture was quickly

introduced into the IR cell while holding the catalyst at 523 K. During the reaction, the gas phase was monitored by recording IR spectra (32 scans) every 30 s. The concentrations of reactants and products were estimated using the absorbance intensities of their characteristic vibration modes as follows: ν(C–O) at 1056 cm^{-1} for ethanol, ν(H–C=O) at 2705 cm^{-1} for acetaldehyde, ν(C–H) at 3016 cm^{-1} for methane, ν(C=O) at 2358 cm^{-1} for CO$_2$, ν(C≡O) at 2170 cm^{-1} for CO, and ν(H–O–H) at 1558 cm^{-1} for water. The detailed calibration procedures have been reported in our previous work [13].

For 1,3-butadiene hydrogenation, the initial ratio of hydrogen to 1,3-butadiene was 2.2:1. The hydrogenation reaction proceeded at a catalyst temperature of 308 K and initial pressure of ~13.0 Torr. The concentrations of reactant and products were estimated using the absorbance intensities of their characteristic vibration modes as follows: ν(C=C–C=C) at 1586 cm^{-1} for 1,3-butadiene, ν(C=C) at 1655 cm^{-1} for 1-butene, and γ(CH$_3$) at 1466 cm^{-1} for butane. Because of peak overlap with 1-butene at 1466 cm^{-1}, the concentration of butane could not be directly determined. Instead, it was estimated by subtracting the 1-butene contribution from the total intensity at 1466 cm^{-1}.

2.3. Analysis of the reaction data

To compare the trends in catalyst activity, the consumption reactions for both ethanol reforming and 1,3-butadiene hydrogenation were approximated as first order. The data analysis procedures have been reported in our previous work [13]. Notable deactivation was found with some catalysts, especially Ni monometallic catalysts. Therefore, deactivation was also included in the rate law. By fitting the measured concentration of the reactant, both the reaction and deactivation rate constants could be obtained simultaneously.

3. Results and discussion

3.1. EXAFS

Analysis of the Pt L$_{III}$-edge X-ray absorption near-edge structure (XANES) and EXAFS can provide information about the oxidation states of the metals and the presence of bimetallic bonds, respectively [15]. Figure 1(a) shows the Pt L$_{III}$-edge XANES spectra of a Pt foil and the six supported Pt-Ni catalysts. All the catalysts exhibited a white line feature prior to reduction that indicates the metal is oxidized; however, following reduction in hydrogen, this white line feature was greatly decreased in all cases, and appeared very similar to the white line of the Pt foil, indicating that the Pt in these catalysts was now in the metallic state. The reduction of Pt is observed in Fig. 1(b), which displays the Fourier transformed EXAFS before and after reduction. The characteristic peak of Pt-O at low radial distribution ($R < 2$ Å) in the fresh samples was no longer present after reduction in hydrogen, and only Pt-M peaks at slightly larger radial distribution (2Å $< R <$ 3 Å) were observed in the EXAFS.

The experimental data after reduction in H$_2$ were fitted using FEFF6 [16] in R-space for the six supported bimetallic Pt-Ni catalysts. The k-ranges used in the fitting were chosen in order to exclude regions of noise at high-k. Some data sets were inherently noisier due to the greater absorptivity of heavier elements such as Ti, Zr, and Ce, which attenuated the X-ray signal. A Hanning window with sill width of 2 Å^{-1} was used in Fourier-transforming the spectra into R-space. The best-fit results are summarized in Table 1. In the bulk phases, Ni and Pt had first-nearest-neighbor distances of 2.492 Å (Ni-Ni) and 2.774 Å (Pt-Pt). For the Pt/Ni bimetallic catalysts, the first-nearest-neighbor distance should be a value in between those for the

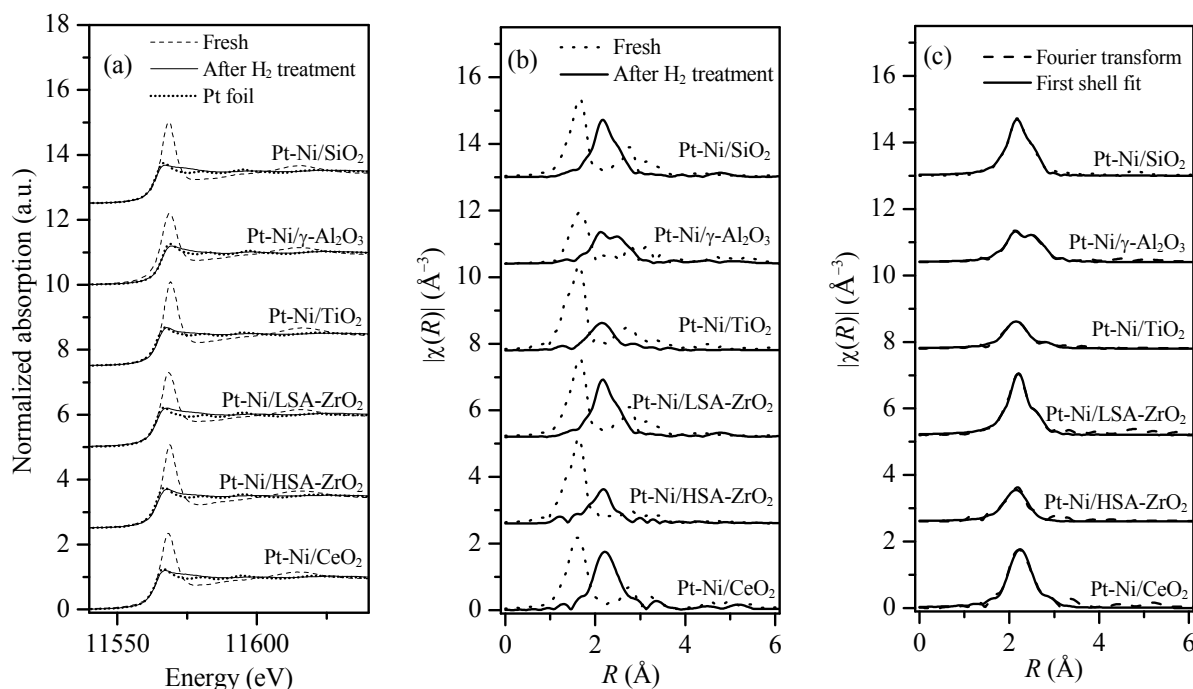**Fig. 1.** Pt LIII-edge XANES spectra (a), Fourier transformed (magnitude) k^2-weighted EXAFS function $|\chi(k)|$ of Pt LIII-edge before and after reduction (b), and first shell fits of $|\chi(k)|$ after reduction (c) for the Pt-Ni bimetallic catalysts on the different supports.

Table 1
Results of Pt L$_{III}$-edge EXAFS analysis and TEM measurements.

Catalyst	Shell	CN	R (Å)	Average particle size from TEM (nm)
Pt-Ni/γ-Al$_2$O$_3$	Pt-Pt	5.7 ± 0.9	2.72 ± 0.01	1.9
	Pt-Ni	3.2 ± 0.5	2.58 ± 0.01	
Pt-Ni/TiO$_2$	Pt-Pt	4.4 ± 2.0	2.70 ± 0.03	1.9
	Pt-Ni	2.8 ± 0.9	2.54 ± 0.01	
Pt-Ni/SiO$_2$	Pt-Pt	3.1 ± 0.4	2.69 ± 0.01	2.1
	Pt-Ni	5.3 ± 0.3	2.57 ± 0.01	
Pt-Ni/HSA-ZrO$_2$	Pt-Pt	1.4 ± 1.8	2.66 ± 0.05	—
	Pt-Ni	4.2 ± 0.9	2.52 ± 0.01	
Pt-Ni/LSA-ZrO$_2$	Pt-Pt	3.1 ± 1.1	2.71 ± 0.01	—
	Pt-Ni	5.8 ± 0.6	2.56 ± 0.01	
Pt-Ni/CeO$_2$	Pt-Pt	2.5 ± 0.4	2.71 ± 0.01	1.8
	Pt-Ni	5.9 ± 0.5	2.56 ± 0.01	

two monometallic distances. As shown in Table 1, the Pt-Ni distance was between 2.54 and 2.58 Å for all the bimetallic catalysts, confirming the formation of the Pt-Ni bonds.

The extent of bimetallic formation appeared to be different on the different supports. The Pt-Ni coordination numbers were found to be 3.2 ± 0.5 on γ-Al$_2$O$_3$, 5.3 ± 0.3 on SiO$_2$, 2.8 ± 0.9 on TiO$_2$, 4.2 ± 0.9 on HSA-ZrO$_2$, 5.8 ± 0.6 on LSA-ZrO$_2$, and 5.9 ± 0.5 on CeO$_2$. The ratio of the Pt-Ni to Pt-Pt coordination numbers characterized the extent of bimetallic bond formation. For the Pt-Ni bimetallic catalysts supported on SiO$_2$, ZrO$_2$, and CeO$_2$, this ratio of coordination numbers was greater than one, signifying that most Pt atoms are primarily coordinated with Ni atoms. In comparison, the ratios for the γ-Al$_2$O$_3$ and TiO$_2$ supported catalysts were less than one, suggesting that the first coordination shell around each Pt atom consisted of more Pt atoms than Ni on these two supports. It is important to note that all these results were obtained in reducing environments. Under reaction conditions, the surface configuration can be altered by the presence of adsorbates [17].

3.2. TEM analysis of particle size distributions

TEM was used to determine the particle size distributions of the reduced bimetallic catalysts. To maximize the contrast between the metal and the support, high-angle annular dark field (HAADF) imaging was used to image the catalysts. The statistics of the particle size distributions, estimated by measuring horizontal particle diameters in several different images for each catalyst, are shown in Table 1. The average particle sizes were very similar for the Pt-Ni bimetallic catalysts over various oxide supports.

3.3. CO uptake

CO uptake results are shown in Table 2. The amount of adsorbed CO provides a quantitative comparison of the number of active sites on the catalysts. The data in Table 2 show that both Pt and Ni monometallic catalysts adsorbed CO at room temperature. Pt-Ni/TiO$_2$ had much lower CO uptake than the other bimetallic catalysts. Because the particle size estimated from TEM measurements was similar on TiO$_2$ and other supports, the difference in the CO uptake was not caused by differences in dispersion, but was instead attributed to the strong metal support interaction (SMSI) effect [18,19]. The Ni monometallic catalysts had smaller CO uptake values than the Pt monometallic and Pt-Ni bimetallic catalysts over the same oxide support.
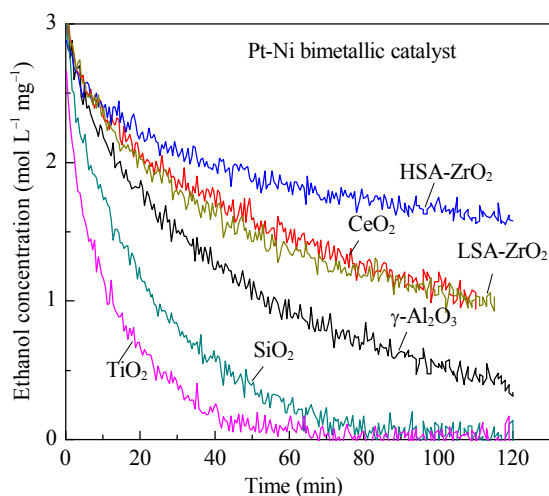
3.4. Effect of support on ethanol reforming

3.4.1. Pt-Ni bimetallic catalysts

The consumption curves for ethanol on the Pt-Ni bimetallic catalysts with different supports at 523 K are shown in Fig. 2. The effect of support was significant, with higher activity seen on TiO$_2$ and SiO$_2$. The catalysts also showed varied stability. For example, the conversion of ethanol over Pt-Ni/HSA-ZrO$_2$ was very similar to that over Pt-Ni/CeO$_2$ and Pt-Ni/LSA-ZrO$_2$ in the first 10 min but became much slower in the subsequent period, indicating that Pt-Ni/HSA-ZrO$_2$ had worse stability than

Table 2
CO uptake and reaction and deactivation rate constants for the different catalysts.

Catalyst	CO uptake (μmol^{-1} g$_{cat}^{-1}$)	Ethanol reforming			1,3-Butadiene hydrogenation		
		k_r (min^{-1} g$_{cat}^{-1}$)	k_d (10^{-3} min^{-1})	Normalized k_r (10^{-2} min^{-1} μmol$_{CO}^{-1}$)	k_r (min^{-1} g$_{cat}^{-1}$)	k_d (10^{-3} min^{-1})	Normalized k_r (10^{-2} min^{-1} μmol$_{CO}^{-1}$)
Pt-Ni/γ-Al$_2$O$_3$	44.4	0.84	7.4	1.88	3.41	13.2	7.85
Pt-Ni/CeO$_2$	35.4	0.55	14.5	1.55	2.93	9.6	8.29
Pt-Ni/HSA-ZrO$_2$	47.1	0.49	51.9	1.04	0.09	0	0.19
Pt-Ni/SiO$_2$	23.6	1.63	2.7	6.93	5.66	0	24.0
Pt-Ni/TiO$_2$	12.8	2.35	2.5	18.39	0.10	0	0.81
Pt-Ni/LSA-ZrO$_2$	40.9	0.80	32.3	1.96	0.99	0	2.42
Pt/γ-Al$_2$O$_3$	45.0	1.96	10.6	4.35	1.40	0	3.21
Pt/CeO$_2$	14.1	0.34	16.0	2.38	0.17	2.2	1.20
Pt/ZrO$_2$(HSA)	40.1	0.34	37.6	0.85	0.09	1.7	0.22
Pt/SiO$_2$	30.7	0.42	21.7	1.36	3.26	21.8	10.6
Pt/TiO$_2$	31.1	1.17	6.7	3.76	0.08	0	0.32
Pt/ZrO$_2$(LSA)	26.2	1.63	9.7	6.21	0.29	0.70	1.11
Ni/γ-Al$_2$O$_3$	14.4	0.78	56.3	5.42	0.78	16.2	5.44
Ni/CeO$_2$	11.2	0.36	41.4	3.23	2.03	10.1	18.2
Ni/HSA-ZrO$_2$	5.1	0.01	15.2	0.27	0.002	0	0.05
Ni/SiO$_2$	10.2	0.08	3.3	0.81	2.43	0	23.9
Ni/TiO$_2$	12.1	0.20	18.1	1.62	0.04	0	0.30
Ni/LSA-ZrO$_2$	15.0	0.25	57.4	1.65	0.42	23.1	2.83

Fig. 2. Comparison of ethanol consumption over Pt-Ni bimetallic catalysts on different supports.

Fig. 3. Effect of supports on activity and stability of the Pt-Ni bimetallic catalysts for ethanol reforming.

Pt-Ni/CeO$_2$ or Pt-Ni/LSA-ZrO$_2$.

For quantitative comparison, the reaction rate k_r and deactivation rate k_d are shown in Fig. 3. The order of activity of the bimetallic catalysts was TiO$_2$ > SiO$_2$ > γ-Al$_2$O$_3$ ≈ LSA-ZrO$_2$ > CeO$_2$ > HSA-ZrO$_2$, and their stabilities were in the order TiO$_2$ ≈ SiO$_2$ > γ-Al$_2$O$_3$ > CeO$_2$ > LSA-ZrO$_2$ > HSA-ZrO$_2$. Overall, the Pt-Ni/TiO$_2$ bimetallic catalyst was the best for reforming ethanol, both in terms of activity and stability. Although the γ-Al$_2$O$_3$-supported catalysts have been intensively studied for aqueous phase reforming of biomass-derived molecules [20], their hydrothermal stability is a significant issue at relatively high temperatures in the aqueous phase [21]. Hydrothermal stability is also a concern for SiO$_2$-supported catalysts. In recent years, there has been progress in improving the thermal and hydrothermal stability of TiO$_2$ [22,23], which makes TiO$_2$ an attractive support for reforming reactions.

Selectivity of H$_2$ production is an important parameter for reforming reactions. Because the vibration modes in gas-phase H$_2$ could not be observed with FT-IR spectroscopy, the production of H$_2$ was determined indirectly through the rates of production of CO and CO$_2$. In the reforming reaction, CO was produced first, followed by CO$_2$ production via the water-gas shift (WGS) reaction. Thus, the concentrations of CO and CO$_2$ could also provide information on the catalyst activity for the WGS reaction. Of the three most active catalysts, i.e. Pt-Ni/TiO$_2$, Pt-Ni/SiO$_2$, and Pt-Ni/γ-Al$_2$O$_3$, Pt-Ni/SiO$_2$ exhibited the greatest CO production, while Pt-Ni/TiO$_2$ displayed the highest CO$_2$ production. Note that with the Pt-Ni/TiO$_2$ catalyst, the CO concentration decreased after 60 min. This was because no CO was produced via reforming reaction during this period, while CO was consumed by the WGS reaction. Although the Pt-Ni/CeO$_2$ catalyst did not show high activity towards the reforming reaction, the production of CO$_2$ was similar to that on Pt-Ni/TiO$_2$, indicating that Pt-Ni/CeO$_2$ had a high activity for the WGS reaction.

Besides the reforming and WGS reactions, dehydrogenation and decomposition reactions were also observed. The selectivities of production of CH$_4$ and acetaldehyde are also compared in Fig. 4. Among the three most active catalysts, the Pt-Ni/SiO$_2$ catalyst possessed the highest selectivity for CH$_4$, while Pt-Ni/TiO$_2$ produced much less CH$_4$. Acetaldehyde is an important intermediate product formed by dehydrogenation of ethanol [24], an important reaction that has drawn much attention in recent years [25]. Pt-Ni/LSA-ZrO$_2$ had the highest selectivity for acetaldehyde, while Pt-Ni/SiO$_2$ had the lowest selectivity. With Pt-Ni/TiO$_2$, the concentration of acetaldehyde was relatively high in the initial period and then decreased by further decomposition. With Pt-Ni/γ-Al$_2$O$_3$ and Pt-Ni/CeO$_2$, the concentration of acetaldehyde remained unchanged during the reaction time studied, indicating that the formation and consumption rates of acetaldehyde were similar. These results suggested that Pt-Ni/TiO$_2$ and Pt-Ni/LSA-ZrO$_2$ had higher dehydrogenation activity to form acetaldehyde compared with the C–C bond scission activity needed to form CO and CH$_4$.
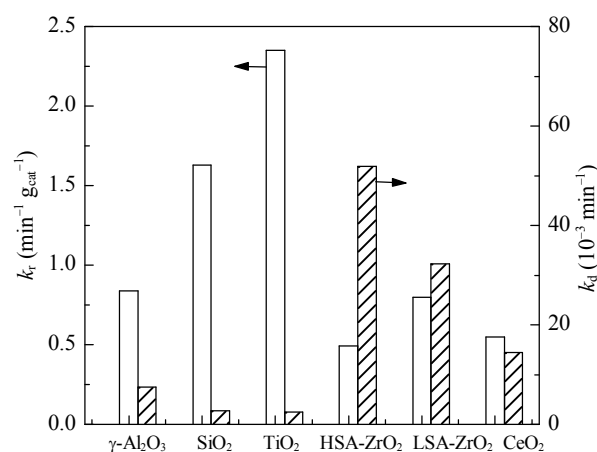
3.4.2. Comparison of bimetallic and monometallic catalysts

To further study the effects of support on reforming of ethanol, the Pt-Ni bimetallic catalysts were compared with Pt and Ni monometallic catalysts in Fig. 5 and Table 2. The activities of the Pt monometallic catalysts were in the order γ-Al$_2$O$_3$ > LSA-ZrO$_2$ ≈ TiO$_2$ > SiO$_2$ ≈ CeO$_2$ ≈ HSA-ZrO$_2$, and the order of stabilities was TiO$_2$ > γ-Al$_2$O$_3$ ≈ LSA-ZrO$_2$ > CeO$_2$ > SiO$_2$ > HSA-ZrO$_2$. Overall, Pt/γ-Al$_2$O$_3$ was the best monometallic catalyst for reforming of ethanol considering both activity and stability. The effects of supports on performance of the Pt-Ni bimetallic catalyst and the Pt monometallic catalysts were different. Synergetic effects were observed on SiO$_2$, TiO$_2$, and HSA-ZrO$_2$ in terms of the rate constants normalized for both catalyst weight and CO uptake. In contrast, the Pt-Ni bimetallic catalyst had a lower activity than the Pt monometallic catalysts on the CeO$_2$, γ-Al$_2$O$_3$, and LSA-ZrO$_2$ supports. The Pt-Ni/TiO$_2$ and Pt-Ni/SiO$_2$ catalysts showed slower deactivation than Pt/TiO$_2$ and Pt/SiO$_2$, especially on the SiO$_2$ support, while Pt-Ni/ZrO$_2$ showed faster deactivation than Pt/ZrO$_2$. The deactivation behavior of the Pt-Ni bimetallic catalysts supported on γ-Al$_2$O$_3$ and CeO$_2$ was similar to that of their corresponding Pt monometallic catalysts.
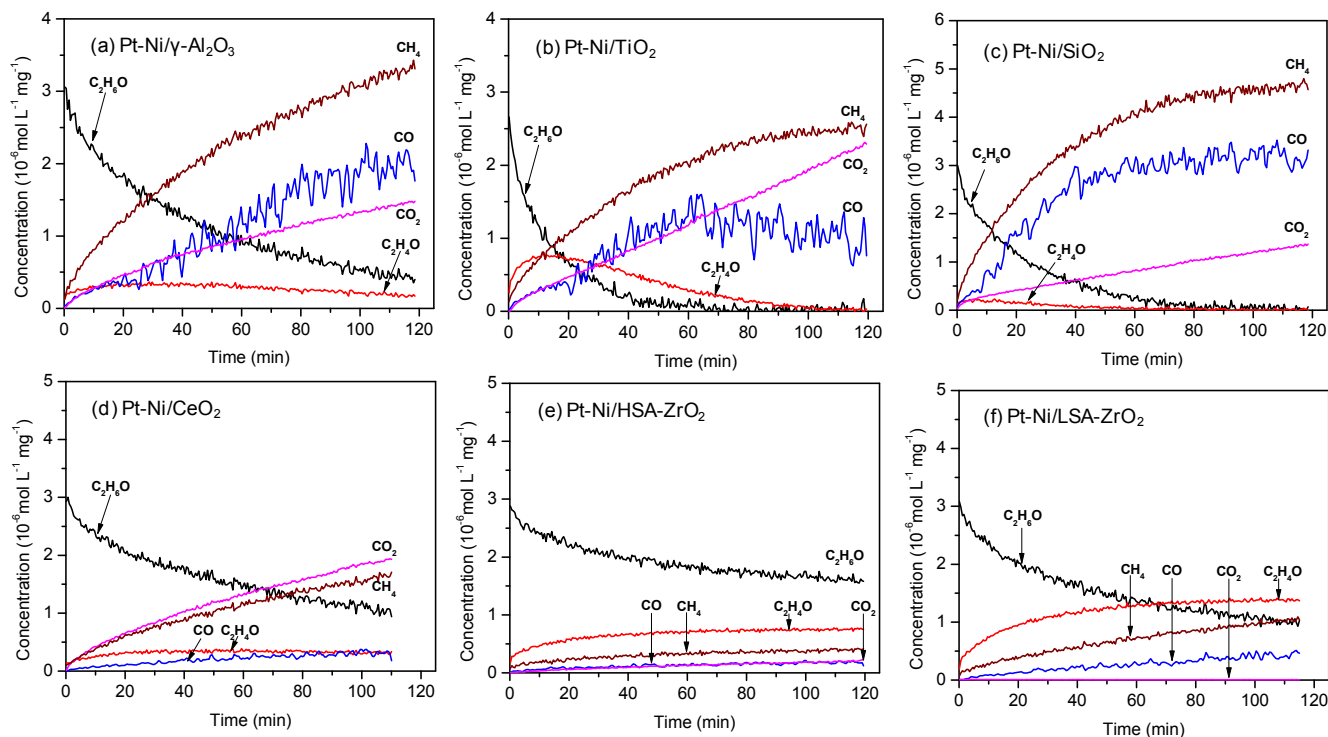
Fig. 4. Effect of supports on the production of CH_4 and acetaldehyde from ethanol reforming.

The monometallic Ni catalysts showed low activity, as shown in Fig. 5 and Table 2. Significant deactivation was observed due to coke deposition during ethanol steam reforming [26]. Experiments on well-defined Pt-Ni single crystal surfaces have shown that the activity of reforming follows the trend NiPtPt(111) > Ni(111) > Pt(111) > PtNiPt(111) [8]. To compare with these results, the reaction rate constants normalized with respect to CO uptake are listed in Table 2. Most Ni catalysts had higher normalized activity than Pt catalysts. Dada also found poor dispersion of Ni on SiO_2, a high reaction rate constant after normalizing for the CO-uptake value, and fast deactivation. Thus, the key issue with the Ni catalyst is to improve its stability and dispersion.

3.5. Effect of support on 1,3-butadiene hydrogenation
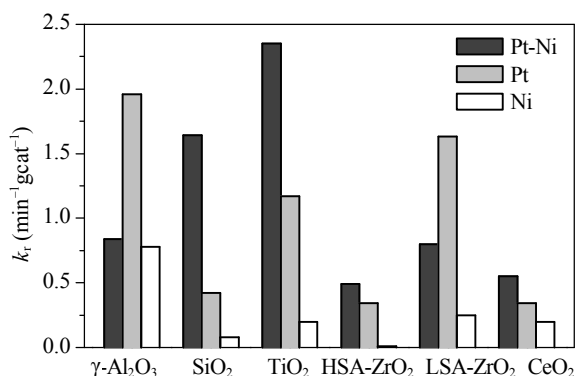
3.5.1. Pt-Ni bimetallic catalysts

Fig. 5. Comparison of the support effects on the activities of PtNi monometallic and bimetallic catalysts for reforming of ethanol.

The hydrogenation of 1,3-butadiene was used as a probe reaction to further study the effect of the oxide support because the substrate that gave the Pt-Ni bimetallic catalyst with the highest activity was different for reforming and hydrogenation. The consumption curves for 1,3-butadiene over the Pt-Ni bimetallic catalysts on different supports at 308 K are shown in Fig. 6, and the rate constants are shown in Fig. 7 and listed in Table 2. There was a significant effect of support on the activity of the catalyst. The activities of the Pt-Ni bimetallic catalysts for hydrogenation of 1,3-butadiene followed the order SiO_2 > CeO_2 > γ-Al_2O_3 > LSA-ZrO_2. The Pt-Ni/TiO_2 and Pt-Ni/HSA-ZrO_2 catalysts were nearly inactive at 308 K. This low activity was probably because of a strong metal-support interaction, which led to formation of Pt-Ni particles with no Pt core [14]. These results
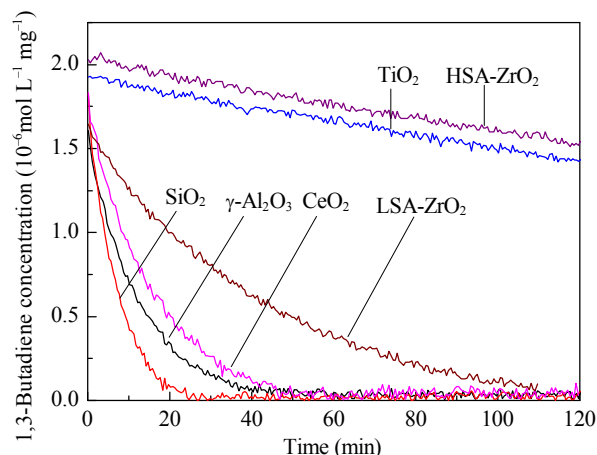

Fig. 6. Consumption of 1,3-butadiene during 1,3-butadiene hydrogenation at 308 K on the Pt-Ni bimetallic catalysts.
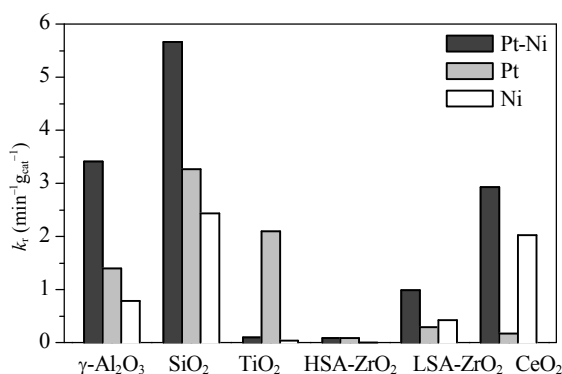
Fig. 7. Comparison of the support effect on the activity of PtNi monometallic and bimetallic catalysts for hydrogenation of 1,3-butadiene.

were consistent with our previous results for hydrogenation of acetone on Pt-Ni bimetallic catalysts on different supports, where the order of activities was $SiO_2 > \gamma$-$Al_2O_3 >> TiO_2$. Among the commonly used supports, SiO_2 was the best for hydrogenation reactions. In contrast with their behavior during the reforming reaction, most catalysts showed little or no deactivation under 1,3-butadiene hydrogenation conditions. This can be at least partially attributed to the low reaction temperature, and thus less carbon deposition.

3.5.2. Comparison of bimetallic and monometallic catalysts

The Pt-Ni bimetallic and monometallic catalysts on different supports are compared in Fig. 7. The activities of the Pt monometallic catalysts for hydrogenation of 1,3-butadiene followed the order $SiO_2 > \gamma$-$Al_2O_3 >> $ LSA-ZrO, CeO_2, TiO_2, HSA-ZrO_2. This trend was similar to that for the Pt-Ni bimetallic catalysts, except that Pt-Ni/CeO_2 and Pt-Ni/LSA-ZrO_2 showed significantly enhanced activity compared to their Pt counterparts. Deactivation was observed with Pt/SiO_2, Pt/CeO_2, Pt/LSA-ZrO_2, and Pt/HSA-ZrO_2. The overall stability of the Pt-Ni bimetallic catalysts was better than that of the corresponding Pt monometallic catalysts.

The overall activity on Ni catalysts was lower than that on the corresponding Pt monometallic or Pt-Ni bimetallic catalysts. The one exception was the Ni/CeO_2 catalyst, which showed a much higher activity than Pt/CeO_2. The activities of the Ni monometallic catalysts for hydrogenation of 1,3-butadiene followed the order $SiO_2 \approx CeO_2 > \gamma$-$Al_2O_3 > $ LSA-ZrO. The Ni/TiO_2 and Ni/HSA-ZrO_2 catalysts showed no activity at 308 K. Deactivation was more pronounced with Ni/γ-Al_2O_3, Ni/CeO_2, and Ni/LSA-ZrO_2, while no deactivation was observed with Ni/SiO_2.

3.6. Discussion

3.6.1. Support effect on reforming reaction

For ethanol reforming, there is a significant synergistic effect for the Pt-Ni bimetallic catalysts on SiO_2 and TiO_2, while Pt-Ni bimetallic catalysts on γ-Al_2O_3 and LSA-ZrO_2 show decreased activity compared to the corresponding Pt monometallic catalysts. This effect is even more pronounced if the rate constants are normalized with respect to CO uptake.

Ultra high vacuum (UHV) experiments and density functional theory (DFT) calculations have shown that the catalytic activity for reforming reactions follows the trend NiPtPt(111) > Ni(111) > Pt(111) > PtNiPt(111) [7,8]. Therefore, one possible reason for the different trends on TiO_2 and SiO_2 compared to those on γ-Al_2O_3 and LSA-ZrO_2 is the differences in configuration of the Pt-Ni bimetallic catalysts on different supports under reforming reaction conditions. It has been shown that oxidizing conditions can make the Ni-terminated, NiPtPt(111) configuration more stable than the Pt-terminated, PtNiPt(111) configuration. The trends found experimentally on a Pt(111) single crystal remain the same, despite the introduction of multiple grain boundaries and crystal planes, when a polycrystalline Pt foil is used [27]. Therefore, the trends predicted and found experimentally for model single crystal surfaces will most likely hold when the model bimetallic systems are extended to nanoparticle catalysts. Grass et al. [28] carried out an in situ study of the interactions of a bimetallic $Rh_{0.5}Pd_{0.5}$ bulk crystal with O_2, CO, and NO using ambient pressure X-ray photoelectron spectroscopy (APXPS) and compared the results to those obtained for 15 nm nanoparticles with the same overall composition. They found that segregation and oxidation/reduction followed the same trend on the bulk crystal as on the nanoparticles but proceeded faster at lower temperature on nanoparticles than on the bulk crystal.

Under the reforming reaction conditions, oxidizing species are present (water and CO_2) which may be adsorbed on the catalyst surface. It is expected that the adsorption of O and/or OH on the surface will pull Ni atoms to the surface. Although the Pt-Ni/γ-Al_2O_3 bimetallic catalyst is less active than Pt/γ-Al_2O_3 for ethanol reforming under the low-pressure studies in this work, different results have been reported for reforming of ethylene glycol in aqueous phase [20]. This suggests that increasing the partial pressure of water may increase the coverage of O and/or OH on the surface and lead to the Ni-terminated bimetallic configuration that is more active for reforming reactions.

The interactions between the oxide support and metal can also affect the surface configuration and catalytic activity. Strong metal-support interaction (SMSI) effects on TiO_2 have been found after high temperature reduction in H_2, resulting in suppressed chemisorption because of the presence of TiO_x species on the metal surface [18,19]. TiO_x on the metal surface of Pt-Ni nanoparticles may cause Ni to segregate to the surface and form NiO_x, since it is expected that Ni atoms will be stable on the catalyst surface in the presence of oxidizing species [4]. In our previous work [13], we used DFT calculations to study the interaction between the Pt-Ni cluster and the support (γ-Al_2O_3 and TiO_2) and found that the binding of Pt or Ni is weaker to TiO_2 than to γ-Al_2O_3. This makes it easier for Ni to segregate to the bimetallic surface on TiO_2 in the presence of adsorbed oxidative species.

3.6.2. Support effect on hydrogenation reaction

In general, the Pt-Ni bimetallic catalysts outperformed the Pt and Ni monometallic catalysts for 1,3-butadiene hydrogenation on all the supports studied, based on equal catalyst weight.

This is consistent with the previous results for benzene and 1,3-butadiene hydrogenation over γ-Al$_2$O$_3$-supported Pt-Ni bimetallic catalysts [9], and acetone hydrogenation with Pt-Ni bimetallic catalysts supported on γ-Al$_2$O$_3$, TiO$_2$ and SiO$_2$ [11].

Note that Pt-Ni bimetallic catalysts have a similar or sometimes smaller number of surface active sites than the corresponding monometallic Pt catalysts, as shown by the CO uptake values. Thus, the enhanced activity of the Pt-Ni bimetallic catalysts is not caused by an increase in the number of active sites. The enhanced hydrogenation activities are consistent with previous surface science studies [29,30] and DFT calculations [31] of low-temperature hydrogenation of cyclohexene on Ni/Pt(111) bimetallic surfaces. In these studies the Pt-terminated bimetallic surface, PtNiPt(111), showed significantly higher hydrogenation activity than the Ni and Pt monometallic surfaces. The higher hydrogenation activity was attributed to the relatively weak binding energies of both atomic hydrogen and cyclohexene on the bimetallic surfaces, leading to facile hydrogenation of cyclohexene. It is also necessary for the Pt-terminated configuration to be stable under the hydrogenation conditions for high hydrogenation reactivity to occur. From previous DFT calculations, the PtNiPt(111) configuration is thermodynamically more stable than the corresponding NiPtPt(111) configuration in vacuum and in the presence of adsorbed atomic hydrogen [4]. Of the six supports evaluated, SiO$_2$ has a weak interaction with the Pt-Ni metal particles, which should favor the formation of a thermodynamically stable Pt-terminated configuration in the Pt-Ni bimetallic particles; this is consistent with the high hydrogenation activity of this catalyst.

4. Conclusions

Ethanol reforming and 1,3-butadiene hydrogenation reactions on Pt-Ni bimetallic and Pt and Ni monometallic catalysts supported on γ-Al$_2$O$_3$, SiO$_2$, TiO$_2$, ZrO$_2$, and CeO$_2$ have been studied. The oxide supports strongly affect the activity of the Pt-Ni monometallic and bimetallic catalysts for both ethanol reforming and 1,3-butadiene hydrogenation, and the optimal support is different for reforming and hydrogenation reactions. For ethanol reforming, the order of activity for Pt-Ni bimetallic catalysts is TiO$_2$ > SiO$_2$ > γ-Al$_2$O$_3$ $\approx$ LSA-ZrO$_2$ > CeO$_2$ > HSA-ZrO$_2$, and the stabilities are TiO$_2$ $\approx$ SiO$_2$ > γ-Al$_2$O$_3$ > CeO$_2$ > LSA-ZrO$_2$ > HSA-ZrO$_2$. In contrast, for 1,3-butadiene hydrogenation, the activity follows the trend of SiO$_2$ > CeO$_2$ > γ-Al$_2$O$_3$ > LSA-ZrO$_2$ > HSA-ZrO$_2$ $\approx$ TiO$_2$. The Pt-Ni bimetallic catalysts outperform the corresponding Pt and Ni monometallic catalysts for 1,3-butadiene hydrogenation, indicating that the Pt-terminated bimetallic configuration is dominant under hydrogenation conditions. For ethanol reforming, Pt-Ni bimetallic catalysts outperform the monometallic catalysts on SiO$_2$, TiO$_2$, HSA-ZrO$_2$, and CeO$_2$ but not on γ-Al$_2$O$_3$ or LSA-ZrO$_2$; this is most likely because of the combined effect of the metal-support interaction and adsorbate-stabilized configuration of the bimetallic catalyst.

References

[1] Sinfelt J H. Bimetallic Catalysts: Discoveries, Concepts, and Applications. New York: Wiley, 1983
[2] Chen J G, Menning C A, Zellner M B. *Surf Sci Rep*, 2008, 63: 201
[3] Yu W T, Porosoff M D, Chen J G. *Chem Rev*, 2012, 112: 5780
[4] Menning C A, Hwu H H, Chen J G. *J Phys Chem B*, 2006, 110: 15471
[5] Murillo L E, Goda A M, Chen J G. *J Am Chem Soc*, 2007, 129: 7101
[6] Skoplyak O, Barteau M A, Chen J G. *ChemSusChem*, 2008, 1: 524
[7] Skoplyak O, Barteau M A, Chen J G. *Surf Sci*, 2008, 602: 3578
[8] Skoplyak O, Barteau M A, Chen J G. *J Phys Chem B*, 2006, 110: 1686
[9] Lonergan W W, Vlachos D G, Chen J G. *J Catal*, 2010, 271: 239
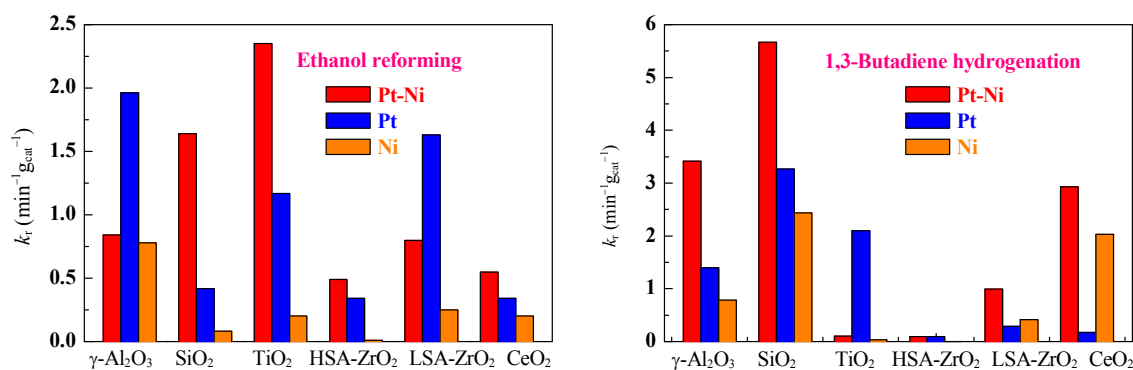[10] Qi S T, Yu W T, Lonergan W W, Yang B, Chen J G. *ChemCatChem*,

---

Graphical Abstract

Selection of oxide supports to anchor desirable bimetallic structures for ethanol reforming and 1,3-butadiene hydrogenation

TiefengWang*, William Lonergan, Jingguang G. Chen*
Tsinghua University, China; University of Delaware, USA; Columbia University, USA

For ethanol reforming, the Pt-Ni bimetallic catalyst activity is in the order TiO$_2$ > SiO$_2$ > γ-Al$_2$O$_3$ $\approx$ LSA-ZrO$_2$ > CeO$_2$ > HSA-ZrO$_2$; while for 1,3-butadiene hydrogenation, the activity follows the trend of SiO$_2$ > CeO$_2$ > γ-Al$_2$O$_3$ > LSA-ZrO$_2$ > HSA-ZrO$_2$ $\approx$ TiO$_2$.

2010, 2: 625

[11] Qi S T, Cheney B A, Zheng R Y, Lonergan W W, Yu W T, Chen J G. *Appl Catal A*, 2011, 393: 44

[12] Menezes A O, Rodrigues M T, Zimmaro A, Borges L E P, Fraga M A. *Renew Energy*, 2011, 36: 595

[13] Wang T F, Mpourmpakis G, Lonergan W W, Vlachos D G, Chen J G. *Phys Chem Chem Phys*, 2013,15: 12156

[14] Lonergan W W, Wang T F, Vlachos D G, Chen J G. *Appl Catal A*, 2011, 408: 87

[15] Jentys A, McHugh B J, Haller G L, Lercher J A. *J Phys Chem*, 1992, 96: 1324

[16] Rehr J J, Albers R C. *Rev Mod Phys*, 2000, 72: 621

[17] Tupy S A, Karim A M, Bagia C, Deng W H, Huang Y L, Vlachos D G, Chen J G. *ACS Catal*, 2012, 2: 2290

[18] Vannice M A, Sudhakar C. *J Phys Chem*, 1984, 88: 2429

[19] Tauster S J, Fung S C, Garten R L. *J Am Chem Soc*, 1987, 100: 170

[20] Huber G W, Shabaker J W, Evans S T, Dumesic J A. *Appl Catal B*,

2006, 62: 226

[21] Rinaldi R, Schueth F. *Energy Environ Sci*, 2009, 2: 610

[22] Cedeno L, Zanella R, Ramirez J, Mendoza H, Hernandez G, Schacht P. *Catal Today*, 2004, 98: 83

[23] Wang D H, Choi D, Yang Z G, Viswanathan V V, Nie Z M, Wang C M, Song Y J, Zhang J G, Liu J. *Chem Mater*, 2008, 20: 3435

[24] Bichon P, Haugom G, Venvik H J, Holmen A, Blekkan E A, *Top Catal*, 2008, 49: 38

[25] Gong J L, Mullins C B. *J Am Chem Soc*, 2008, 130: 16458

[26] Fatsikostas A N, Kondarides D I, Verykios X E. *Catal Today*, 2002, 75: 145

[27] Menning C A, Chen J G. *Top Catal*, 2010, 53: 338

[28] Grass M E, Park M, Aksoy F, Zhang Y W, Kunz M, Liu Z, Mun B S. *Langmuir*, 2010, 26: 16362

[29] Hwu H H, Eng J Jr, Chen J G. *J Am Chem Soc*, 2002, 124: 702

[30] Khan N A, Murillo L E, Chen J G. *J Phys Chem B*, 2004, 108: 15748

[31] Humbert M P, Murillo L E, Chen J G. *ChemPhysChem*, 2008, 9: 1262

选择氧化物载体调变乙醇重整和1,3-丁二烯加氢反应双金属催化剂

王铁峰[a,*], William Lonergan[b], 陈经广[c,#]

[a]清华大学化工系, 绿色反应工程与工艺北京市重点实验室, 北京100084, 中国
[b]特拉华大学化学与生物分子工程系, 催化科技中心, 纽瓦克DE 19716, 美国
[c]哥伦比亚大学化工系, 纽约NY 10027, 美国

摘要: 研究了不同载体负载的Pt-Ni双金属和单金属催化剂上乙醇重整和1,3-丁二烯加氢反应性能, 以考察氧化物载体对双金属结构和催化活性的影响. 所用的氧化物载体包括γ-Al$_2$O$_3$, SiO$_2$, TiO$_2$, CeO$_2$以及高比表面积(HSA)和低比表面积(LSA)ZrO$_2$. 采用共浸渍法制备催化剂, 用CO化学吸附、透射电镜和扩展X射线吸收精细结构光谱进行催化剂表征, 采用傅里叶变换红外间歇反应器进行化学反应评价. 对于乙醇重整反应, Pt-Ni双金属催化剂优于单金属催化剂, Pt-Ni双金属催化剂活性顺序为TiO$_2$ > SiO$_2$ > γ-Al$_2$O$_3$ ≈ LSA-ZrO$_2$ > CeO$_2$ > HSA-ZrO$_2$. 对于1,3-丁二烯加氢反应, 在SiO$_2$, TiO$_2$和HSA-ZrO$_2$载体上双金属催化剂优于单金属催化剂, Pt-Ni双金属催化剂活性顺序为SiO$_2$ > CeO$_2$ > γ-Al$_2$O$_3$ > LSA-ZrO$_2$ > HSA-ZrO$_2$ ≈ TiO$_2$.
关键词: 铂镍双金属催化剂; 载体影响; 乙醇重整; 1,3-丁二烯加氢; 扩展X射线吸收精细结构光谱